International Journal of Solids and Structures 50 (2013) 2667–2677

Contents lists available at SciVerse ScienceDirect

International Journal of Solids and Structures

journal homepage: www.elsevier.com/locate/ijsolstr

Pre-kinking of a moving crack in a magnetoelectroelastic material under in-plane loading

Keqiang Hu *, Zengtao Chen

Department of Mechanical Engineering, University of New Brunswick, Fredericton, New Brunswick, Canada E3B 5A3

ARTICLE INFO

Article history:
Received 20 November 2012
Received in revised form 2 March 2013
Available online 30 April 2013

Keywords:
Constant moving crack
Magnetoelctroelastic material
Dual integral equations
Crack kinking
Hoop stress intensity factor

ABSTRACT

A constant moving crack in a magnetoelectroelastic material under in-plane mechanical, electric and magnetic loading is studied for impermeable crack surface boundary conditions. Fourier transform is employed to reduce the mixed boundary value problem of the crack to dual integral equations, which are solved exactly. Steady-state asymptotic fields near the crack tip are obtained in closed form and the corresponding field intensity factors are expressed explicitly. The crack speed influences the singular field distribution around the crack tip and the effects of electric and magnetic loading on the crack tip fields are discussed. The crack kinking phenomena is investigated using the maximum hoop stress intensity factor criterion. The magnitude of the maximum hoop stress intensity factor tends to increase as the crack speed increases.

1. Introduction

Composite materials consisting of piezoelectric and piezomagnetic phases exhibit magnetoelectric effect unavailable in single-phase piezoelectric or piezomagnetic materials. Owing to the unique magneto-electro-elastic coupling effect, these materials can be used in intelligent structures as sensors and actuators. Study on the properties of piezoelectric/piezomagnetic composites has drawn considerable attention in recent years. Some defects (such as dislocations and cracks) could be induced during the manufacturing processes or during service by the mechanical, electric or magnetic loading, which can adversely influence the performance of the structures. Therefore, it is necessary to advance our understanding of the characteristics of magnetoelectroelastic material with defects.

In recent decades, there is a growing interest among researchers in solving fracture mechanics problems in magnetoelectroelastic media. Crack initiation behavior in a magnetoelectroelastic composite under in-plane deformation was investigated by Song and Sih (2003). Gao et al. (2003) developed an exact treatment on the crack problems in a magnetoelectroelastic solid subjected to far-field loading. Qin (2005) obtained 2D Green's functions of defective magnetoelectroelastic solids under thermal loading, which can be used to establish boundary element formulation and to analyze relevant fracture problems. Li (2005) made the transient analysis of a cracked magnetoelectroelastic medium under antiplane mechanical and inplane electric and magnetic impacts. The dynamic response of a penny-shaped crack in a magnetoelectroelastic layer was studied by Feng et al. (2007). Boundary element method was developed by Rojas-Díaz et al. (2007) to study crack problems in linear magnetoelectroelastic materials under static loading conditions. Wang and Mai (2007) discussed the different electromagnetic boundary conditions on the crack-faces in magnetoelectroelastic materials with coupled piezoelectric, piezomagnetic and magnetoelectric effects. Zhong and Li (2007) gave a magnetoelectroelastic analysis for an opening crack in a piezoelectromagnetic solid. Zhou and Chen (2008) analyzed a partially conducting mode I crack in piezoelectromagnetic materials. Zhao and Fan (2008) proposed a strip electric–magnetic breakdown model in magnetoelectroelastic medium to study the nonlinear character of electric field and magnetic field on fracture of magnetoelectroelastic materials. The problem of a planar magnetoelectroelastic layered half-plane subjected to generalized line forces and edge dislocations was analyzed by Ma and Lee (2009). Li and Lee (2010) established real fundamental solutions for in-plane magnetoelectroelastic governing equations and studied collinear unequal cracks in magnetoelectroelastic materials. An embedded mixed-mode crack in a functionally graded magnetoelectroelastic infinite medium has been studied by Rekik et al. (2012). Wan et al. (2012) investigated a mode III crack crossing the magneto-electroelastic biomaterial interface under concentrated magneto-electromechanical loads.

Theoretical investigation of crack propagation in elastic material begins with Yoffe (1951) analysis of the near-tip field of a constant moving crack, and subsequent investigations were carried

* Corresponding author. Tel./fax: +1 506 458 7104.
E-mail addresses: ckhu@unb.ca, keqianghu@163.com (K. Hu).

0020-7683/$ - see front matter © 2013 Elsevier Ltd. All rights reserved.
http://dx.doi.org/10.1016/j.ijsolstr.2013.04.016

out by Craggs (1960), Freund (1972), Willis (1967), Frund (1990), Yang et al. (1991), among others. Gao (1993) proposed a wavy-crack model to explain important discrepancies between theory and experiments, and the analysis indicates that the basic mechanism of dynamic branching is somewhat like a thermally activated kinetic process.

Considering the coupling effect of mechanical and electrical fields, Li and Mataga (1996a,b) investigated the dynamic anti-plane crack propagation in piezoelectric materials. The moving crack problem in a piezoelectric material under longitudinal shear has been studied by Chen and Yu (1997), Chen et al. (1998), Li et al. (2000), and Kwon and Lee (2001), etc. Hu and Zhong (2005) considered a moving mode-III crack in a functionally graded piezoelectric strip and showed that the gradient of the material properties can affect the magnitudes of the stress intensity factors. Under the assumption of in-plane electro-mechanical loading, the moving crack problems in a piezoelectric material have been investigated by Soh et al. (2002), Herrmann and Loboda (2006) and Piva et al. (2007), among others.

The moving crack problem in an infinite magnetoelectroelastic body under anti-plane shear and in-plane electro-magnetic loading has recently been solved by Hu and Li (2005a) whose results predicted that the moving crack may curve when the speed of the crack is greater than a certain value. Tian and Rajapakse (2008) presented a theoretical study for crack branching in magnetoelectroelastic solids by extending the generalized dislocation model. The moving crack at the interface between dissimilar magnetoelectroelastic materials under anti-plane shear has been investigated by Hu et al. (2006). Tupholme (2009) studied a moving anti-plane shear crack in transversely isotropic magnetoelectroelastic media when subjected to representative non-constant crack-face loading conditions.

To the best knowledge of the authors, the problem of a moving crack in a magnetoelectroelastic material under in-plane magneto-electro-mechanical loading has not been reported in the literature. This problem is solved in this paper. Fourier transforms are applied and the mixed boundary value problem of the crack is reduced to solving dual integral equations, which are solved exactly. The asymptotic fields near the crack tip are obtained in a closed form and the corresponding field intensity factors are expressed explicitly. By applying the criterion of maximum hoop stress intensity factors, the crack kinking phenomenon is investigated. The coupling magneto-electro-elastic effects on the crack-tip fields are studied and the influence of crack speed on the dynamic fracture property is discussed.

2. Basic equations for magnetoelectroelastic material

Consider a transversely isotropic, linear magnetoelectroelastic material and denote the rectangular coordinates of a point by $x_j (j = 1, 2, 3)$. The dynamic equilibrium equations are:

$$\sigma_{ij,i} = \rho \frac{\partial^2 u_j}{\partial t^2}, \quad D_{i,i} = 0, \quad B_{i,i} = 0 \tag{1}$$

where body forces and free charges are neglected, σ_{ij}, D_i and B_i are components of stress, electrical displacement and magnetic induction, respectively; ρ is the mass density of the magnetoelctroelastic material; a comma followed by i ($i = 1, 2, 3$) denotes partial differentiation with respect to the coordinate x_i, and the usual summation convention over repeated indices is applied. The constitutive equations can be written as

$$\begin{aligned} \sigma_{ij} &= C_{ijks}\varepsilon_{ks} - e_{sij}E_s - h_{sij}H_s \\ D_i &= e_{iks}\varepsilon_{ks} + \lambda_{is}E_s + d_{is}H_s \\ B_i &= h_{iks}\varepsilon_{ks} + d_{is}E_s + \mu_{is}H_s \end{aligned} \tag{2}$$

where ε_{ks}, E_s and H_s are components of strain, electric field and magnetic field, respectively; C_{ijks}, e_{iks}, h_{iks} and d_{is} are elastic, piezoelectric, piezomagnetic and electromagnetic constants, respectively; λ_{is} and μ_{is} are dielectric permittivities and magnetic permeabilities, respectively. The following reciprocal symmetries hold:

$$\begin{aligned} &C_{ijks} = C_{jiks} = C_{ijsk} = C_{ksij}, \ e_{sij} = e_{sji} \\ &h_{sij} = h_{sji}, \ d_{ij} = d_{ji}, \ \lambda_{ij} = \lambda_{ji}, \ \mu_{ij} = \mu_{ji} \end{aligned} \tag{3}$$

The gradient equations are

$$\varepsilon_{ij} = \frac{1}{2}(u_{i,j} + u_{j,i}), \quad E_i = -\phi_{,i}, \quad H_i = -\varphi_{,i} \tag{4}$$

where u_i is the displacement vector, ϕ and φ are the electric and magnetic potentials, respectively.

Under the assumption of plane strain, the constitutive equations take the form as (Huang and Kuo, 1997):

$$\begin{aligned} \begin{Bmatrix} \sigma_{11} \\ \sigma_{33} \\ \sigma_{13} \end{Bmatrix} &= \begin{bmatrix} C_{11} & C_{13} & 0 \\ C_{13} & C_{33} & 0 \\ 0 & 0 & C_{44} \end{bmatrix} \begin{Bmatrix} u_{1,1} \\ u_{3,3} \\ u_{1,3} + u_{3,1} \end{Bmatrix} + \begin{bmatrix} 0 & e_{31} \\ 0 & e_{33} \\ e_{15} & 0 \end{bmatrix} \begin{Bmatrix} \phi_{,1} \\ \phi_{,3} \end{Bmatrix} \\ &\quad + \begin{bmatrix} 0 & h_{31} \\ 0 & h_{33} \\ h_{15} & 0 \end{bmatrix} \begin{Bmatrix} \varphi_{,1} \\ \varphi_{,3} \end{Bmatrix} \\ \begin{Bmatrix} D_1 \\ D_3 \end{Bmatrix} &= \begin{bmatrix} 0 & 0 & e_{15} \\ e_{31} & e_{33} & 0 \end{bmatrix} \begin{Bmatrix} u_{1,1} \\ u_{3,3} \\ u_{1,3} + u_{3,1} \end{Bmatrix} - \begin{bmatrix} \lambda_{11} & 0 \\ 0 & \lambda_{33} \end{bmatrix} \begin{Bmatrix} \phi_{,1} \\ \phi_{,3} \end{Bmatrix} \\ &\quad - \begin{bmatrix} d_{11} & 0 \\ 0 & d_{33} \end{bmatrix} \begin{Bmatrix} \varphi_{,1} \\ \varphi_{,3} \end{Bmatrix} \\ \begin{Bmatrix} B_1 \\ B_3 \end{Bmatrix} &= \begin{bmatrix} 0 & 0 & h_{15} \\ h_{31} & h_{33} & 0 \end{bmatrix} \begin{Bmatrix} u_{1,1} \\ u_{3,3} \\ u_{1,3} + u_{3,1} \end{Bmatrix} - \begin{bmatrix} d_{11} & 0 \\ 0 & d_{33} \end{bmatrix} \begin{Bmatrix} \phi_{,1} \\ \phi_{,3} \end{Bmatrix} \\ &\quad - \begin{bmatrix} \mu_{11} & 0 \\ 0 & \mu_{33} \end{bmatrix} \begin{Bmatrix} \varphi_{,1} \\ \varphi_{,3} \end{Bmatrix} \end{aligned} \tag{5}$$

The governing equations can be written as:

$$\begin{aligned} &C_{11}u_{1,11} + C_{44}u_{1,33} + (C_{13} + C_{44})u_{3,13} + (e_{31} + e_{15})\phi_{,13} \\ &\quad + (h_{31} + h_{15})\varphi_{,13} = \rho u_{1,tt} \\ &(C_{13} + C_{44})u_{1,13} + C_{44}u_{3,11} + C_{33}u_{3,33} + e_{15}\phi_{,11} + e_{33}\phi_{,33} \\ &\quad + h_{15}\varphi_{,11} + h_{33}\varphi_{,33} = \rho u_{3,tt} \\ &(e_{31} + e_{15})u_{1,13} + e_{15}u_{3,11} + e_{33}u_{3,33} - \lambda_{11}\phi_{,11} - \lambda_{33}\phi_{,33} - d_{11}\varphi_{,11} \\ &\quad - d_{33}\varphi_{,33} = 0 \\ &(h_{31} + h_{15})u_{1,13} + h_{15}u_{3,11} + h_{33}u_{3,33} - d_{11}\phi_{,11} - d_{33}\phi_{,33} - \mu_{11}\varphi_{,11} \\ &\quad - \mu_{33}\varphi_{,33} = 0 \end{aligned} \tag{6}$$

3. Problem statement and method of solution

Consider a Griffith crack of length $2c$ moving at a constant speed v in the magnetoelectroelastic material, with the poling direction as the x_3-axis, as shown in Fig. 1. Uniform normal stress P_0, in-plane electric field E_0 and magnetic field H_0 are applied at the infinity.

For convenience, let a Cartesian coordinate system (x, y, z) be attached to the moving crack and when $t = 0$ it coincides with the fixed coordinate system (x_1, x_2, x_3). Since the problem is in a steady state, the Galilean transformation can be introduced, i.e.,

$$x = x_1 - vt, \quad y = x_2, \quad z = x_3 \tag{7}$$

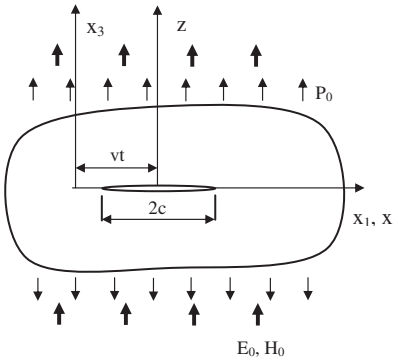

Fig. 1. A cracked magnetoelectroelastic material under in-plane mechanical, electric and magnetic loading.

With reference to the moving coordinate system (x, y, z), the governing Eq. (6) become independent of the time variable t and may be rewritten as

$$\begin{aligned}
&(C_{11}-\rho v^2)u_{x,xx}+C_{44}u_{x,zz}+(C_{13}+C_{44})u_{z,xz}+(e_{31}+e_{15})\phi_{,xz}\\
&\quad+(h_{31}+h_{15})\varphi_{,xz}=0\\
&(C_{13}+C_{44})u_{x,xz}+(C_{44}-\rho v^2)u_{z,xx}+C_{33}u_{z,zz}+e_{15}\phi_{,xx}+e_{33}\phi_{,zz}\\
&\quad+h_{15}\varphi_{,xx}+h_{33}\varphi_{,zz}=0\\
&(e_{31}+e_{15})u_{x,xz}+e_{15}u_{z,xx}+e_{33}u_{z,zz}-\lambda_{11}\phi_{,xx}-\lambda_{33}\phi_{,zz}\\
&\quad-d_{11}\varphi_{,xx}-d_{33}\varphi_{,zz}=0\\
&(h_{31}+h_{15})u_{x,xz}+h_{15}u_{z,xx}+h_{33}u_{z,zz}-d_{11}\phi_{,xx}-d_{33}\phi_{,zz}-\mu_{11}\varphi_{,xx}\\
&\quad-\mu_{33}\varphi_{,zz}=0
\end{aligned} \tag{8}$$

As shown in Fig. 1, symmetry arguments are used to allow for consideration of only the first quadrant with appropriate conditions along the coordinate axes. The corresponding boundary conditions of the mixed boundary value problem are:

$$\sigma_{zz}(x,\infty)=P_0,\quad \sigma_{zx}(x,\infty)=0 \tag{9}$$

$$E_z(x,\infty)=E_0,\quad H_z(x,\infty)=H_0 \tag{10}$$

$$\sigma_{xz}(x,0)=0 \tag{11}$$

$$\sigma_{zz}(x,0)=0,\quad (0\leqslant x<c) \tag{12-1}$$

$$u_z(x,0)=0\quad (x\geqslant c) \tag{12-2}$$

Considering the fact that the electric and magnetic constants of magnetoelectroelastic materials are large and are on the order of a few thousand times the electric and magnetic permittivities of air or vacuum inside the crack, the impermeable electric and magnetic boundary conditions along the crack face can be assumed (Hu and Li, 2005b). It is noted that the impermeable crack face condition is one of the extreme cases of actual crack face boundary conditions, which are also related to the real crack openings (Zhao et al., 2006a,b). The mixed boundary conditions for the magneto-electrically impermeable crack are:

$$\phi(x,0)=0,\quad \varphi(x,0)=0\quad (x\geqslant c) \tag{13}$$

$$D_z(x,0)=0,\quad B_z(x,0)=0\quad (0\leqslant x<c) \tag{14}$$

Fourier transforms are then applied on Eq. (8) and the results are

$$u_x(x,z)=\sum_{j=1}^{4}a_j\gamma_j\int_0^\infty A_j(\xi)\exp(-\gamma_j\xi z)\sin(\xi x)d\xi \tag{15-1}$$

$$u_z(x,z)=\sum_{j=1}^{4}\int_0^\infty A_j(\xi)\exp(-\gamma_j\xi z)\cos(\xi x)d\xi+\Pi_1 z \tag{15-2}$$

$$\phi(x,z)=-\sum_{j=1}^{4}b_j\int_0^\infty A_j(\xi)\exp(-\gamma_j\xi z)\cos(\xi x)d\xi+\Pi_2 z \tag{15-3}$$

$$\varphi(x,z)=-\sum_{j=1}^{4}d_j\int_0^\infty A_j(\xi)\exp(-\gamma_j\xi z)\cos(\xi x)d\xi+\Pi_3 z \tag{15-4}$$

where $\Pi_j (j=1,2,3)$ are constants and a_j, b_j, d_j $(j=1,2,3,4)$ are known coefficients defined in Appendix A, $A_j(\xi), (j=1,2,3,4)$ are unknowns to be determined and γ_j $(j=1,2,3,4)$ are the roots of the following characteristic equation

$$|\mathbf{M}|=\begin{vmatrix}
C_{11}-\rho v^2-C_{44}\gamma^2 & (C_{13}+C_{44})\gamma & (e_{31}+e_{15})\gamma & (h_{31}+h_{15})\gamma\\
(C_{13}+C_{44})\gamma & C_{33}\gamma^2+\rho v^2-C_{44} & e_{33}\gamma^2-e_{15} & h_{33}\gamma^2-h_{15}\\
(e_{31}+e_{15})\gamma & e_{33}\gamma^2-e_{15} & \lambda_{11}-\lambda_{33}\gamma^2 & d_{11}-d_{33}\gamma^2\\
(h_{31}+h_{15})\gamma & h_{33}\gamma^2-h_{15} & d_{11}-d_{33}\gamma^2 & \mu_{11}-\mu_{33}\gamma^2
\end{vmatrix}=0 \tag{16}$$

where $|\mathbf{M}|$ denotes the determinant of the matrix $\mathbf{M}$.

Note that the eighth-order characteristic equation (16) has eight roots which occur in pairs with the same magnitude but opposite signs, and for complex roots, the roots they always appear in conjugate pairs. In the expressions (15), the roots γ_j $(j=1,2,3,4)$ are chosen as $\mathrm{Re}(\gamma_j)>0$ by requiring a positive internal energy for the system to be in a steady state, as stated by Stroh (1962) and Suo et al. (1992).

The limiting speed can be obtained by setting one of the roots vanishes, which leads to the characteristic equation:

$$\begin{aligned}
&(C_{11}-\rho v^2)[(\lambda_{11}\mu_{11}-d_{11}^2)(\rho v^2-C_{44})+e_{15}(d_{11}h_{15}-\mu_{11}e_{15})\\
&\quad+h_{15}(d_{11}e_{15}-\lambda_{11}h_{15})]=0
\end{aligned} \tag{17}$$

which gives two limiting speeds as:

$$\begin{aligned}
&V_L=\sqrt{\frac{C_{11}}{\rho}},\quad V_T=\sqrt{\frac{\mu}{\rho}}\\
&\mu=C_{44}+\frac{\mu_{11}e_{15}^2+\lambda_{11}h_{15}^2-2d_{11}e_{15}h_{15}}{\lambda_{11}\mu_{11}-d_{11}^2}
\end{aligned} \tag{18}$$

where V_L and V_T are the longitudinal wave speed and transverse wave speed of magnetoelectroelastic materials, respectively. In our present study, the crack speed is less than the transverse wave speed V_T, i.e., in the range of subsonic regime.

The expressions for the stresses, electric displacement and magnetic induction can be obtained as follows:

$$\sigma_{xz}=-\sum_{j=1}^{4}f_j\int_0^\infty \xi A_j(\xi)\exp(-\gamma_j\xi z)\sin(\xi x)d\xi \tag{19-1}$$

$$\sigma_{zz}=P_0+\sum_{j=1}^{4}h_j\int_0^\infty \xi A_j(\xi)\exp(-\gamma_j\xi z)\cos(\xi x)d\xi \tag{19-2}$$

$$\sigma_{xx}=\sigma_0+\sum_{j=1}^{4}g_j\int_0^\infty \xi A_j(\xi)\exp(-\gamma_j\xi z)\cos(\xi x)d\xi \tag{19-3}$$

$$D_z=D_0+\sum_{j=1}^{4}m_j\int_0^\infty \xi A_j(\xi)\exp(-\gamma_j\xi z)\cos(\xi x)d\xi \tag{20-1}$$

$$D_x=-\sum_{j=1}^{4}s_j\int_0^\infty \xi A_j(\xi)\exp(-\gamma_j\xi z)\sin(\xi x)d\xi \tag{20-2}$$

$$B_z = B_0 + \sum_{j=1}^{4} n_j \int_0^\infty \xi A_j(\xi) \exp(-\gamma_j \xi z) \cos(\xi x) d\xi \tag{21-1}$$

$$B_x = -\sum_{j=1}^{4} t_j \int_0^\infty \xi A_j(\xi) \exp(-\gamma_j \xi z) \sin(\xi x) d\xi \tag{21-2}$$

where σ_0, D_0, B_0 are constants defined in Appendix A and the coefficients are defined as:

$$\begin{aligned} f_j &= C_{44}(a_j\gamma_j^2 + 1) - e_{15}b_j - h_{15}d_j \\ h_j &= (C_{13}a_j + e_{33}b_j + h_{33}d_j - C_{33})\gamma_j \\ g_j &= (C_{11}a_j + e_{31}b_j + h_{31}d_j - C_{13})\gamma_j \\ m_j &= (e_{31}a_j - \lambda_{33}b_j - d_{33}d_j - e_{33})\gamma_j \\ n_j &= (h_{31}a_j - d_{33}b_j - \mu_{33}d_j - h_{33})\gamma_j \\ s_j &= e_{15}(a_j\gamma_j^2 + 1) + \lambda_{11}b_j + d_{11}d_j \\ t_j &= h_{15}(a_j\gamma_j^2 + 1) + d_{11}b_j + \mu_{11}d_j \qquad (j = 1,2,3,4) \end{aligned} \tag{22}$$

By substituting the solution (19)–(21) into the boundary conditions (9)–(11), it is shown that Eqs. (9) and (10) are satisfied completely, and the following relations can be observed:

$$\sum_{j=1}^{4} f_j A_j(\xi) = 0 \tag{23}$$

The unknown $A_4(\xi)$ can be expressed as the three independent unknown functions $A_j(\xi)$ (j = 1,2,3) as:

$$A_4(\xi) = -[f_1A_1(\xi) + f_2A_2(\xi) + f_3A_3(\xi)]/f_4 \tag{24}$$

Satisfaction of the mixed boundary conditions (12–14) on the crack face line leads to the dual integral equations as follows:

$$\int_0^\infty \xi \sum_{j=1}^{3} T_{1j} A_j(\xi) \cos(\xi x) d\xi = -P_0, (0 \leqslant x < c) \tag{25-1}$$

$$\int_0^\infty \sum_{j=1}^{3} R_{1j} A_j(\xi) \cos(\xi x) d\xi = 0, \quad (x \geqslant c) \tag{25-2}$$

$$\int_0^\infty \xi \sum_{j=1}^{3} T_{2j} A_j(\xi) \cos(\xi x) d\xi = -D_0, \quad (0 \leqslant x < c) \tag{26-1}$$

$$\int_0^\infty \sum_{j=1}^{3} R_{2j} A_j(\xi) \cos(\xi x) d\xi = 0, \quad (x \geqslant c) \tag{26-2}$$

$$\int_0^\infty \xi \sum_{j=1}^{3} T_{3j} A_j(\xi) \cos(\xi x) d\xi = -B_0, \quad (0 \leqslant x < c) \tag{27-1}$$

$$\int_0^\infty \sum_{j=1}^{3} R_{3j} A_j(\xi) \cos(\xi x) d\xi = 0, \quad (x \geqslant c) \tag{27-2}$$

where T_{ij}, $R_{ij}(i,j = 1,2,3)$ are known functions defined, respectively, as:

$$\begin{aligned} T_{1j} &= (f_4h_j - f_jh_4)/f_4 \\ T_{2j} &= (f_4m_j - f_jm_4)/f_4 \\ T_{3j} &= (f_4n_j - f_jn_4)/f_4 \quad (j = 1,2,3) \end{aligned} \tag{28}$$

$$\begin{aligned} R_{1j} &= 1 - f_j/f_4 \\ R_{2j} &= (f_4b_j - f_jb_4)/f_4 \\ R_{3j} &= (f_4d_j - f_jd_4)/f_4 \quad (j = 1,2,3) \end{aligned} \tag{29}$$

The simultaneous dual integral equations can be further expressed in the following simple form as:

$$\int_0^\infty \xi A_j(\xi) \cos(\xi x) d\xi = X_j, \quad (0 \leqslant x < c) \quad (j = 1,2,3) \tag{30-1}$$

$$\int_0^\infty A_j(\xi) \cos(\xi x) d\xi = 0, \quad (x \geqslant c) \quad (j = 1,2,3) \tag{30-2}$$

where constants X_j, $(j = 1,2,3)$ are defined as

$$\begin{Bmatrix} X_1 \\ X_2 \\ X_3 \end{Bmatrix} = -\begin{bmatrix} T_{11} & T_{12} & T_{13} \\ T_{21} & T_{22} & T_{23} \\ T_{31} & T_{32} & T_{33} \end{bmatrix}^{-1} \begin{Bmatrix} P_0 \\ D_0 \\ B_0 \end{Bmatrix} \tag{31}$$

Obviously, we can get the analytical solution of the standard dual integral equations (30) as (Copson, 1961)

$$A_j(\xi) = X_j \frac{c \cdot J_1(\xi c)}{\xi}, \quad (j = 1,2,3) \tag{32}$$

where $J_1()$ denotes the first order Bessel function of the first kind.

4. Asymptotic fields near the crack tip

From the point of view of fracture mechanics, only the singular field quantities around the crack tip will be derived here. The singular crack tip fields correspond to the behaviour of the integrand as the integration variables ξ tends to infinity. The stress field, electric field and magnetic field near the crack tip can be obtained by substituting Eqs. (32) and (24) into Eqs. (19)–(21). By considering the identity (Fabrikant, 2003):

$$\int_0^\infty \exp(-\gamma_j z\xi) J_1(\xi c) \sin(x\xi) d\xi = \frac{1}{c}\left[\frac{l_{1j}\sqrt{c^2 - l_{1j}^2}}{l_{2j}^2 - l_{1j}^2}\right] = \frac{S_{1j}(x,z)}{c} \tag{33-1}$$

$$\int_0^\infty \exp(-\gamma_j z\xi) J_1(\xi c) \cos(x\xi) d\xi = \frac{1}{c}\left[1 - \frac{l_{2j}\sqrt{l_{2j}^2 - c^2}}{l_{2j}^2 - l_{1j}^2}\right] = \frac{S_{2j}(x,z)}{c} \tag{33-2}$$

where

$$\begin{aligned} S_{1j}(x,z) &= \frac{l_{1j}\sqrt{c^2 - l_{1j}^2}}{l_{2j}^2 - l_{1j}^2} \\ S_{2j}(x,z) &= 1 - \frac{l_{2j}\sqrt{l_{2j}^2 - c^2}}{l_{2j}^2 - l_{1j}^2} \quad (j = 1,2,3,4) \end{aligned} \tag{34-1}$$

$$l_{kj} = \frac{1}{2}\left[\sqrt{(c+x)^2 + (\gamma_j z)^2} + (-1)^k\sqrt{(c-x)^2 + (\gamma_j z)^2}\right] \quad (k = 1,2; j = 1,2,3,4) \tag{34-2}$$

The stresses, electric displacements and magnetic induction in the cracked magnetoelectroelastic material can be obtained as:

$$\sigma_{zz}(x,z) = P_0 + \sum_{j=1}^{3} X_j \left[h_j S_{2j}(x,z) - \frac{h_4 f_j}{f_4} S_{24}(x,z)\right] \tag{35-1}$$

$$\sigma_{xx}(x,z) = \sigma_0 + \sum_{j=1}^{3} X_j \left[g_j S_{2j}(x,z) - \frac{g_4 f_j}{f_4} S_{24}(x,z)\right] \tag{35-2}$$

$$\sigma_{xz}(x,z) = \sum_{j=1}^{3} f_j X_j [S_{14}(x,z) - S_{1j}(x,z)] \tag{35-3}$$

$$D_z(x,z) = D_0 + \sum_{j=1}^{3} X_j \left[m_j S_{2j}(x,z) - \frac{m_4 f_j}{f_4} S_{24}(x,z) \right] \tag{36-1}$$

$$D_x(x,z) = \sum_{j=1}^{3} X_j \left[\frac{s_4 f_j}{f_4} S_{14}(x,z) - s_j S_{1j}(x,z) \right] \tag{36-2}$$

$$B_z(x,z) = B_0 + \sum_{j=1}^{3} X_j \left[n_j S_{2j}(x,z) - \frac{n_4 f_j}{f_4} S_{24}(x,z) \right] \tag{37-1}$$

$$B_x(x,z) = \sum_{j=1}^{3} X_j \left[\frac{t_4 f_j}{f_4} S_{14}(x,z) - t_j S_{1j}(x,z) \right] \tag{37-2}$$

The asymptotic expressions of the magneto-electro-elastic fields around the crack tip can be determined by introducing a polar coordinate system (r,θ) with the origin at the right crack tip as:

$$r = \sqrt{(x-c)^2 + z^2}, \quad \theta = \tan^{-1}\left(\frac{z}{x-c}\right) \tag{38}$$

Following the procedure in Li and Lee (2004), in the near vicinity of the crack tip, i.e. $r \ll c$, we have

$$l_{kj} \approx c + \frac{r}{2}\left[\cos(\theta) + (-1)^k \sqrt{\cos^2(\theta) + \gamma_j^2 \sin^2(\theta)}\right] \quad (k = 1,2; j = 1,2,3,4) \tag{39}$$

Upon substituting Eq. (39) into Eqs. (35)–(37) and neglecting some higher-order infinitesimal terms, the asymptotic expressions for the magnetoelectroelastic fields in the vicinity of the crack tip are obtained as:

$$\sigma_{zz}(r,\theta) = \sqrt{\frac{c}{2r}} \sum_{j=1}^{3} X_j \left[\frac{h_4 f_j}{f_4} \Lambda_{24}(\theta) - h_j \Lambda_{2j}(\theta) \right] \tag{40-1}$$

$$\sigma_{xx}(r,\theta) = \sqrt{\frac{c}{2r}} \sum_{j=1}^{3} X_j \left[\frac{g_4 f_j}{f_4} \Lambda_{24}(\theta) - g_j \Lambda_{2j}(\theta) \right] \tag{40-2}$$

$$\sigma_{xz}(r,\theta) = \sqrt{\frac{c}{2r}} \sum_{j=1}^{3} f_j X_j [\Lambda_{14}(\theta) - \Lambda_{1j}(\theta)] \tag{40-3}$$

$$D_z(r,\theta) = \sqrt{\frac{c}{2r}} \sum_{j=1}^{3} X_j \left[\frac{m_4 f_j}{f_4} \Lambda_{24}(\theta) - m_j \Lambda_{2j}(\theta) \right] \tag{41-1}$$

$$D_x(r,\theta) = \sqrt{\frac{c}{2r}} \sum_{j=1}^{3} X_j \left[\frac{s_4 f_j}{f_4} \Lambda_{14}(\theta) - s_j \Lambda_{1j}(\theta) \right] \tag{41-2}$$

$$B_z(r,\theta) = \sqrt{\frac{c}{2r}} \sum_{j=1}^{3} X_j \left[\frac{n_4 f_j}{f_4} \Lambda_{24}(\theta) - n_j \Lambda_{2j}(\theta) \right] \tag{42-1}$$

$$B_x(r,\theta) = \sqrt{\frac{c}{2r}} \sum_{j=1}^{3} X_j \left[\frac{t_4 f_j}{f_4} \Lambda_{14}(\theta) - t_j \Lambda_{1j}(\theta) \right] \tag{42-2}$$

where the angular functions $\Lambda_{1j}(\theta)$ and $\Lambda_{2j}(\theta)$ are given as follows:

$$\Lambda_{kj}(\theta) = \sqrt{\frac{\sqrt{\cos^2(\theta) + \gamma_j^2 \sin^2(\theta)} + (-1)^k \cos(\theta)}{2[\cos^2(\theta) + \gamma_j^2 \sin^2(\theta)]}} \quad (k = 1,2;\ j = 1,2,3,4) \tag{43}$$

It can be observed that the stresses, electric displacement and magnetic induction near the crack tip possess the square-root singularity, and the expressions of the angular functions are dependent on the crack speed as the roots of the characteristic Eq. (16) change as the crack speed varies. The angular functions are in agreement with those for static crack problem in piezoelectric and magnetoelectroelastic materials (Lin et al. 2003; Zhong and Li, 2008) when the crack speed vanishes. It should be noted that the crack-tip fields are dependent on the mechanical, electrical and magnetic loading applied in the infinity as considering the relations shown in Eqs. (31) and (35) through (37).

Different criteria have been proposed to predict the direction of crack kinking. Commonly used fracture criteria are the maximum hoop stress intensity factor, the maximum Mode-I stress intensity factor and the maximum energy release rate (Yang, 2002). The prediction based on the energy release rate is greatly different from that based on the stress intensity factor criterion (Azhdari and Nemat-Nasser, 1996a). For anisotropic materials, the hoop stress intensity factor (HSIF) and shear stress intensity factor (SSIF) are more convenient quantities than the commonly used Mode I and II stress intensity factors, since HSIF and SSIF uncouple the Modes I and II on planes at suitable angles relative to the crack (Azhdari and Nemat-Nasser, 1996b).

The hoop and shear stresses at an angle θ near the right tip of the crack are obtained from the following relations in terms of the polar coordinates (r, θ) (Lekhnitskii, 1963):

$$\begin{aligned} \sigma_{\theta\theta} &= \sigma_{zz}\cos^2\theta + \sigma_{xx}\sin^2\theta - \sigma_{zx}\sin 2\theta \\ \sigma_{r\theta} &= \frac{\sigma_{zz} - \sigma_{xx}}{2}\sin 2\theta + \sigma_{zx}\cos 2\theta \end{aligned} \tag{44}$$

Similar definition can be made to the hoop electric displacement and hoop magnetic induction defined in terms of polar coordinates as

$$D_{\theta\theta} = D_z \cos\theta - D_x \sin\theta \tag{45}$$

$$B_{\theta\theta} = B_z \cos\theta - B_x \sin\theta \tag{46}$$

By substituting Eqs. (40) into (44), the hoop stress and shear stress can be expressed as:

$$\sigma_{\theta\theta}(r,\theta) = \sqrt{\frac{c}{2r}} \sum_{j=1}^{3} \frac{X_j}{f_4} \begin{Bmatrix} f_j(h_4\cos^2\theta + g_4\sin^2\theta)\Lambda_{24}(\theta) \\ -f_4(h_j\cos^2\theta + g_j\sin^2\theta)\Lambda_{2j}(\theta) \\ +f_4 f_j[\Lambda_{1j}(\theta) - \Lambda_{14}(\theta)]\sin 2\theta \end{Bmatrix} \tag{47-1}$$

$$\sigma_{r\theta}(r,\theta) = \sqrt{\frac{c}{2r}} \sum_{j=1}^{3} \frac{X_j}{2f_4} \begin{Bmatrix} [f_j(h_4 - g_4)\Lambda_{24}(\theta) + f_4(g_j - h_j)\Lambda_{2j}(\theta)]\sin 2\theta \\ +2f_4 f_j[\Lambda_{14}(\theta) - \Lambda_{1j}(\theta)]\cos 2\theta \end{Bmatrix} \tag{47-2}$$

$$D_{\theta\theta}(r,\theta) = \sqrt{\frac{c}{2r}} \sum_{j=1}^{3} \frac{X_j}{f_4} \begin{Bmatrix} [m_4 f_j \Lambda_{24}(\theta) - m_j f_4 \Lambda_{2j}(\theta)]\cos\theta \\ +[f_4 s_j \Lambda_{1j}(\theta) - f_j s_4 \Lambda_{14}(\theta)]\sin\theta \end{Bmatrix} \tag{48-1}$$

$$D_{rr}(r,\theta) = \sqrt{\frac{c}{2r}} \sum_{j=1}^{3} \frac{X_j}{f_4} \begin{Bmatrix} [m_4 f_j \Lambda_{24}(\theta) - m_j f_4 \Lambda_{2j}(\theta)]\sin\theta \\ +[f_j s_4 \Lambda_{14}(\theta) - f_4 s_j \Lambda_{1j}(\theta)]\cos\theta \end{Bmatrix} \tag{48-2}$$

$$B_{\theta\theta}(r,\theta) = \sqrt{\frac{c}{2r}} \sum_{j=1}^{3} \frac{X_j}{f_4} \begin{Bmatrix} [n_4 f_j \Lambda_{24}(\theta) - n_j f_4 \Lambda_{2j}(\theta)]\cos\theta \\ +[f_4 t_j \Lambda_{1j}(\theta) - f_j t_4 \Lambda_{14}(\theta)]\sin\theta \end{Bmatrix} \tag{48-3}$$

$$B_{rr}(r,\theta) = \sqrt{\frac{c}{2r}} \sum_{j=1}^{3} \frac{X_j}{f_4} \begin{Bmatrix} [n_4 f_j \Lambda_{24}(\theta) - n_j f_4 \Lambda_{2j}(\theta)]\sin\theta \\ +[f_j t_4 \Lambda_{14}(\theta) - f_4 t_j \Lambda_{1j}(\theta)]\cos\theta \end{Bmatrix} \tag{48-4}$$

Define the hoop stress intensity factor and shear stress intensity factor associated with the hoop and shear stresses at an arbitrary angle θ as:

$$K_{\theta\theta} = \lim_{r\to 0}(\sqrt{2r}\sigma_{\theta\theta})$$
$$K_{r\theta} = \lim_{r\to 0}(\sqrt{2r}\sigma_{r\theta}) \tag{49-1}$$

Similarly define the hoop electric displacement intensity factor (HEDIF) and the hoop magnetic induction intensity factor (HMIIF) as follows:

$$K_{D\theta} = \lim_{r\to 0}(\sqrt{2r}D_{\theta\theta})$$
$$K_{B\theta} = \lim_{r\to 0}(\sqrt{2r}B_{\theta\theta}) \tag{49-2}$$

Substituting Eqs. (47) into (49), the hoop and shear stress intensity factors can be obtained as:

$$K_{\theta\theta} = \sqrt{c}\sum_{j=1}^{3}\frac{X_j}{f_4}\left\{\begin{array}{l} f_j(h_4\cos^2\theta + g_4\sin^2\theta)\Lambda_{24}(\theta) \\ -f_4(h_j\cos^2\theta + g_j\sin^2\theta)\Lambda_{2j}(\theta) \\ +f_4f_j[\Lambda_{1j}(\theta) - \Lambda_{14}(\theta)]\sin 2\theta \end{array}\right\} \tag{50-1}$$

$$K_{r\theta} = \sqrt{c}\sum_{j=1}^{3}\frac{X_j}{f_4}\left\{\begin{array}{l} [f_j(h_4 - g_4)\Lambda_{24}(\theta) + f_4(g_j - h_j)\Lambda_{2j}(\theta)]\sin 2\theta \\ +2f_4f_j[\Lambda_{14}(\theta) - \Lambda_{1j}(\theta)]\cos 2\theta \end{array}\right\} \tag{50-2}$$

In this paper, the criteria of maximum hoop stress intensity factor will be applied to predict the possible crack kinking with the assumption that the fracture toughness is same in all directions around the crack. The hoop electric displacement intensity factor (HEDIF) and the hoop magnetic induction intensity factor (HMIIF) are

$$K_{D\theta} = \sqrt{c}\sum_{j=1}^{3}\frac{X_j}{f_4}\left\{\begin{array}{l} [m_4f_j\Lambda_{24}(\theta) - m_jf_4\Lambda_{2j}(\theta)]\cos\theta \\ +[f_4s_j\Lambda_{1j}(\theta) - f_js_4\Lambda_{14}(\theta)]\sin\theta \end{array}\right\} \tag{51-1}$$

$$K_{B\theta} = \sqrt{c}\sum_{j=1}^{3}\frac{X_j}{f_4}\left\{\begin{array}{l} [n_4f_j\Lambda_{24}(\theta) - n_jf_4\Lambda_{2j}(\theta)]\cos\theta \\ +[f_4t_j\Lambda_{1j}(\theta) - f_jt_4\Lambda_{14}(\theta)]\sin\theta \end{array}\right\} \tag{51-2}$$

It is noted that at any angle different form the original crack plane, the hoop stress intensity factor (HSIF), shear stress intensity factor (SSIF), hoop electric displacement intensity factor (HEDIF) and the hoop magnetic induction intensity factor (HMIIF) are

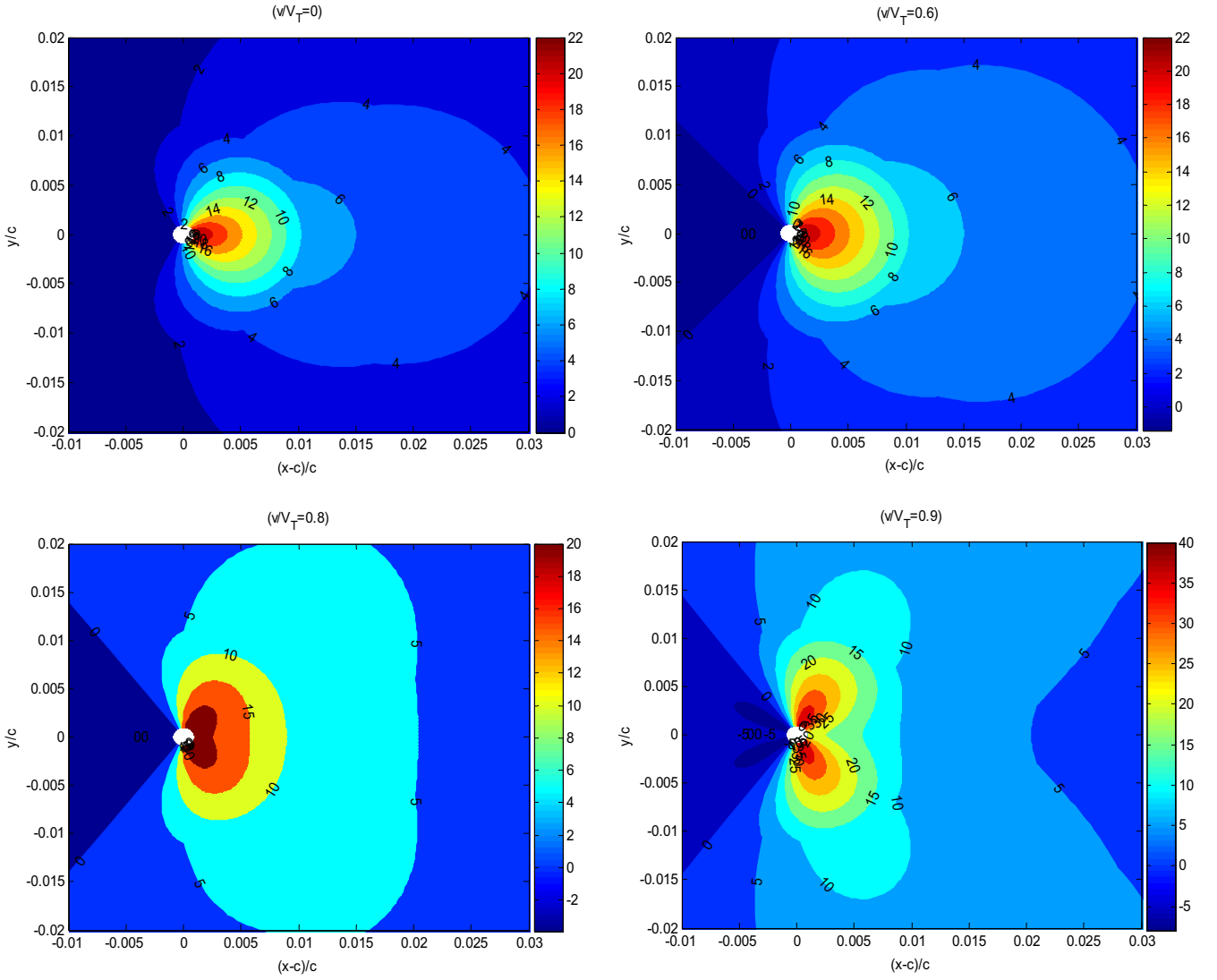

Fig. 2. Dynamic isochromatics of the normalized hoop stress around a moving crack tip when $L_E = L_H = +0.5$.

coupled with each other, as shown in Eqs. (31), (50)–(51). As the angular distribution function of the singular fields near the crack are dependent on the crack speed, the HSIF, SSIF, HEDIF and HMIIF all vary with the crack speed. This conclusion is different from the case of static crack problem.

By setting the angle θ equal to zero and using the relations in Eqs. (43), (28), and (31), the common expressions for the Mode-I and Mode-II stress intensity factors can be obtained as:

$$K_I = K_{\theta\theta}|_{\theta=0} = \sqrt{c}\sum_{j=1}^{3}\frac{X_j}{f_4}(f_j h_4 - f_4 h_j) = P_0\sqrt{c} \tag{52}$$

$$K_{II} = K_{r\theta}|_{\theta=0} = 0 \tag{53}$$

This result shows that the commonly defined stress intensity factor K_I is only dependent on the remote normal stress loading and the mode-II stress intensity is zero.

The electric displacement intensity factor and magnetic induction intensity factor can be defined as:

$$\begin{aligned} K_D &= \lim_{r\to 0}\sqrt{2r}D_z(r,0) = K_{D\theta}|_{\theta=0} = \sqrt{c}\sum_{j=1}^{3}\frac{X_j}{f_4}(m_4 f_j - m_j f_4) \\ &= \sqrt{c}[e_{33}P_0 + (C_{33}\lambda_{33} + e_{33}^2)E_0 + (C_{33}d_{33} + e_{33}h_{33})H_0]/C_{33} \end{aligned} \tag{54}$$

$$\begin{aligned} K_B &= \lim_{r\to 0}\sqrt{2r}B_z(r,0) = K_{B\theta}|_{\theta=0} = \sqrt{c}\sum_{j=1}^{3}X_j\left(\frac{n_4 f_j - n_j f_4}{f_4}\right) \\ &= \sqrt{c}[h_{33}P_0 + (C_{33}d_{33} + e_{33}h_{33})E_0 + (C_{33}\mu_{33} + h_{33}^2)H_0]/C_{33} \end{aligned} \tag{55}$$

It can be observed that the commonly defined electric displacement intensity factor and magnetic induction intensity factor are dependent on the remote normal stress, electric field and magnetic field loadings. These commonly defined field intensity factors are independent of the speed of the moving crack, this conclusion agrees with those for a moving crack in an infinite piezoelectric material (Chen and Yu, 1997; Soh et al., 2002; Piva et al., 2007).

5. Numerical results and discussions

For the magneto-electrically impermeable crack problem, the crack-tip fields are dependent on the remote mechanical, electrical and magnetic loading. To study the effect of magneto-electro-elastic interaction, the electric and magnetic loading parameters are introduced as:

$$L_E = \frac{e_{33}E_0}{P_0}, \quad L_H = \frac{h_{33}H_0}{P_0} \tag{56}$$

The magneto-electro-elastic material is taken to be a transversely isotropic material exhibiting full coupling between electric, electric and magnetic fields, with the polarized direction perpendicular to the crack plane. The material constants of $BaTiO_3$–$CoFe_2O_4$ composite (Tian and Rajapakse, 2005) are used in the following numerical calculation:

$$\begin{aligned} &C_{11} = 22.6\times10^{10}(\mathrm{N/m^2}),\ C_{13} = 12.4\times10^{10}(\mathrm{N/m^2}) \\ &C_{33} = 21.6\times10^{10}(\mathrm{N/m^2}),\ C_{44} = 4.4\times10^{10}(\mathrm{N/m^2}) \\ &e_{15} = 5.8(\mathrm{C/m^2}),\ e_{31} = -2.2(\mathrm{C/m^2}),\ e_{33} = 9.3(\mathrm{C/m^2}) \\ &h_{15} = 275(\mathrm{N/Am}),\ h_{31} = 290.2(\mathrm{N/Am}),\ h_{33} = 350(\mathrm{N/Am}) \\ &\lambda_{11} = 56.4\times10^{-10}(\mathrm{C^2/Nm^2}),\ \lambda_{33} = 63.5\times10^{-10}(\mathrm{C^2/Nm^2}) \\ &\mu_{11} = 29.7\times10^{-5}(\mathrm{Ns^2/C^2}),\ \mu_{33} = 6.35\times10^{-5}(\mathrm{Ns^2/C^2}) \\ &d_{11} = 5.367\times10^{-12}(\mathrm{Ns/VC}),\ d_{33} = 2737.5\times10^{-12}(\mathrm{Ns/VC}) \\ &\rho = 5.7\times10^{3}(\mathrm{kg/m^3}) \end{aligned} \tag{57}$$

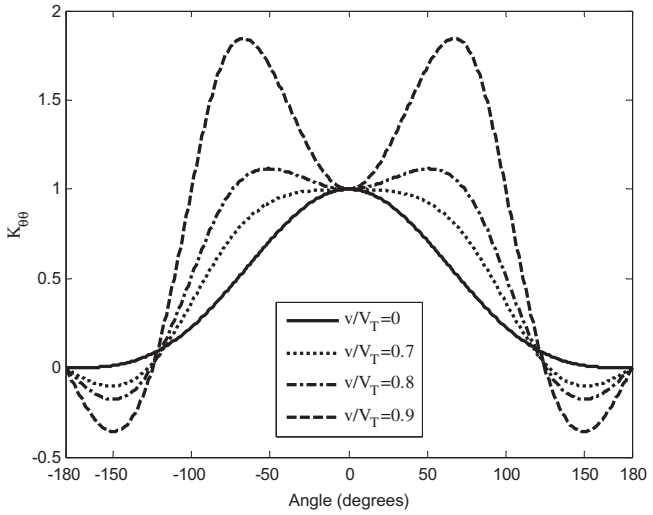

Fig. 3. The normalized HSIFs $K_{\theta\theta}$ versus angle θ for different crack speed when $L_E = L_H = +0.5$.

The dynamic isochromatics of the normalized hoop stress $\frac{\sigma_{\theta\theta}}{P_0\sqrt{c}}$ around the right crack tip for different crack speeds v/V_T are displayed in Fig. 2. Without loss of generality, the applied normal stress is taken to be $P_0 = 4.2$ MPa , the magnitudes of the electric and magnetic loading parameters are chosen as $L_E = +0.5$ and $L_H = +0.5$, respectively. It can be seen from Fig. 2 that the isochromatic fringe loops around crack tip vary as the crack speed changes. It is shown that the maximum hoop stress occurs along the crack line when the crack speed is lower than a certain value (say $v/V_T = 0.7$), which means that the crack has a tendency to propagate along its original plane when the criterion of the maximum hoop stress intensity factor is applied. When the crack speed is higher than a certain value, the maximum hoop stresses occur at some nonzero angles, which indicates that the crack has a tendency to deviate from its original plane if the fracture toughness is assumed to be the same in different directions, and the crack kinking will occur.

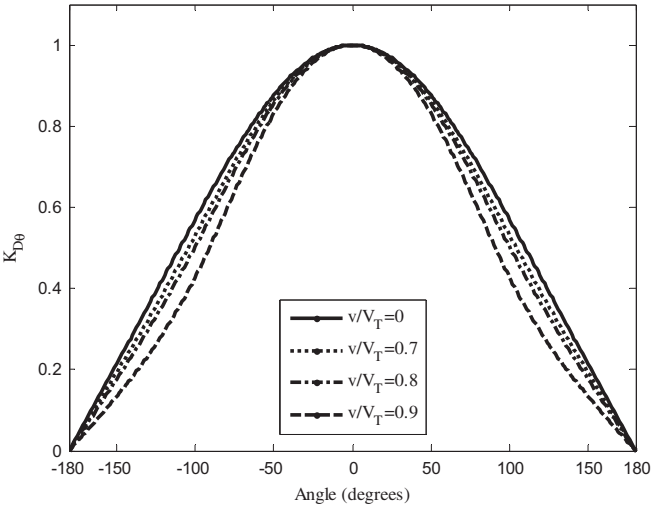

Fig. 4. The normalized HEDIFs $K_{D\theta}$ versus angle θ for different crack speed when $L_E = L_H = +0.5$.

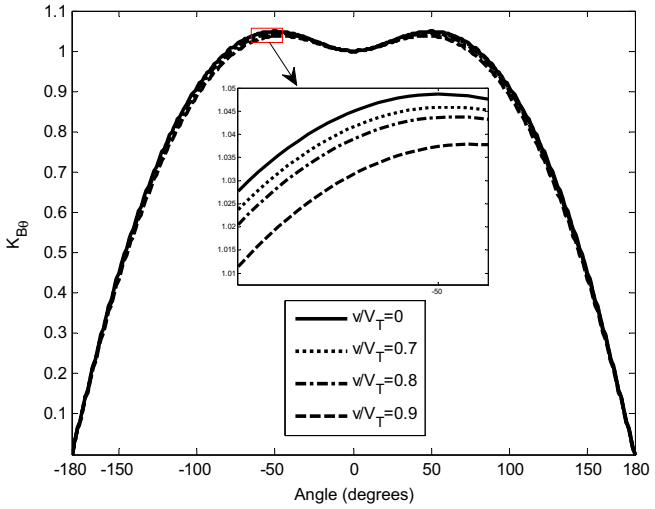

Fig. 5. The normalized HMIIFs $K_{B\theta}$ versus angle θ for different crack speed when $L_E = L_H = +0.5$.

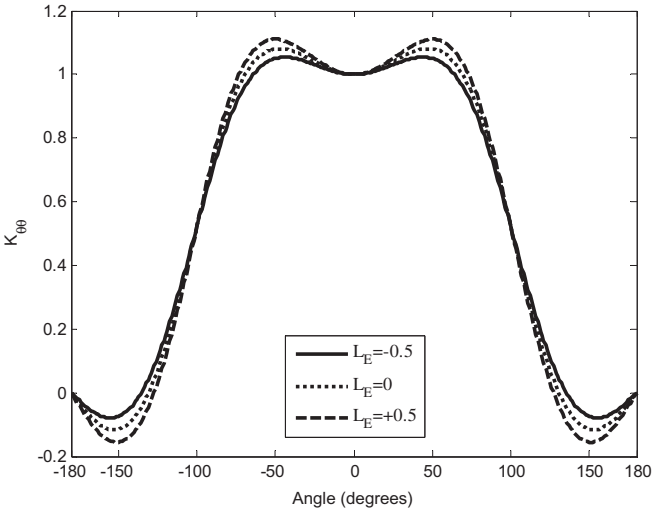

Fig. 6. The normalized HSIFs versus angle θ for different electric loading parameters when $L_H = 0$ and $v/V_T = 0.8$.

Fig. 3 shows the normalized HSIF $\frac{K_{II\theta}}{P_0\sqrt{c}}$ versus angle θ for different crack speed when $L_E = L_H = +0.5$. It shows that the normalized HSIF is 1 when $\theta = 0$, which corresponds to the Mode I stress intensity factor for an infinite, magnetoelectroelastic material. When the crack speed is lower than a certain value ($v/V_T = 0.7$), the maximum HSIF occurs along the crack plane $\theta = 0$. As the crack speed increases, the maximum HSIF increases and moves away from $\theta = 0$ and appears at two symmetric angles, which indicates that the crack may deviate from the original crack plane and propagate along these two symmetric directions.

Fig. 4 shows the normalized HEDIF $\frac{K_{D\theta}}{D_0\sqrt{c}}$ versus angle θ for different crack speed when $L_E = L_H = +0.5$. The value of the normalized HEDIF is 1 when $\theta = 0$, which corresponds to the Mode I electric displacement intensity factor for the impermeable crack in an infinite magnetoelectroelastic material. It also shows that the effect of the crack speed on the variation of the HEDIFs is rather small when $v/V_T \leqslant 0.7$. Fig. 5 displays the variation of normalized HMIIF $\frac{K_{B\theta}}{B_0\sqrt{c}}$ with angle θ for different crack speeds when electromagnetic loading $L_E = L_H = +0.5$ is applied. Along the crack plane $\theta = 0$, the value of the normalized HMIIF is 1, which is the exact solution of the Mode I magnetic induction intensity factor for the impermeable

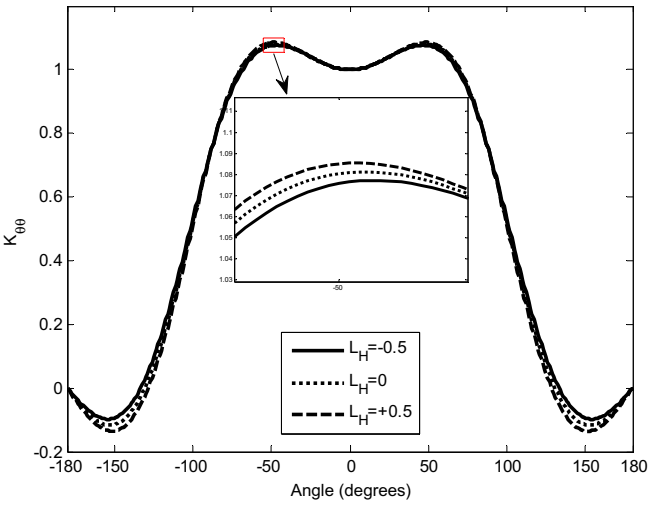

Fig. 7. The normalized HSIFs versus angle θ for different magnetic loading parameters when $L_E = 0$ and $v/V_T = 0.8$.

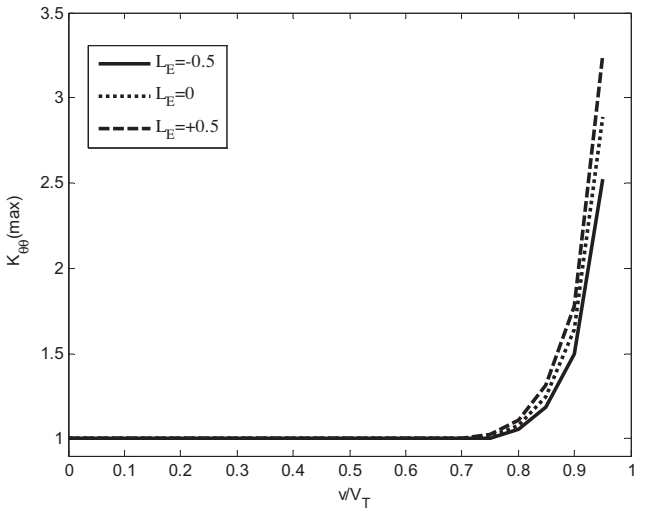

Fig. 8a. The maximum HSIFs versus v/V_T for different electric field loading L_E when $L_H = 0$.

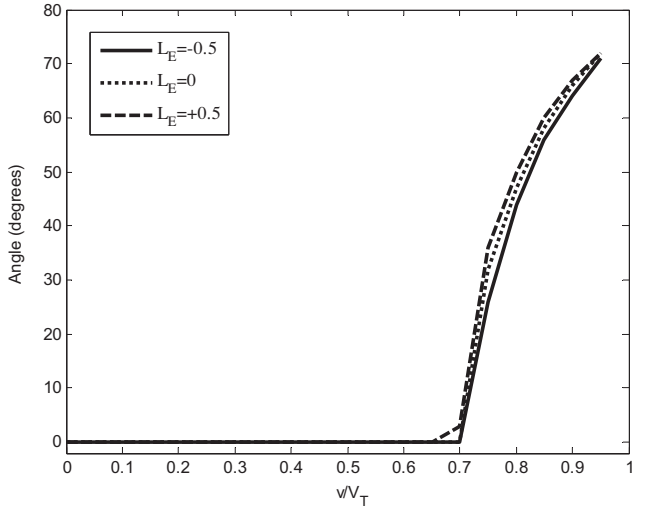

Fig. 8b. The crack kinking angles versus v/V_T for different L_E when $L_H = 0$.

crack in an infinite magnetoelectric material. The influence of the crack speed on the HMIIFs is small when $v/V_T \leqslant 0.7$.

Fig. 6 shows the effect of electric loading parameters on the variation of HSIF with angle when $L_H = 0$ and $v/V_T = 0.8$. The value of the normalized HSIF is 1 when $\theta = 0$, and the magnitude of the HSIF may increase or decrease as the applied electric field loading changes from negative to positive, depending on the different angle orientations around the crack tip. The "negative" means that the direction of the electric and magnetic loading is opposite to the poling direction. It can be observed that the crack has a tendency to propagate along the original crack plane when a negative electric field is applied, and the crack may deviate from the original plane when a positive electric field is applied. The maximum value of the HSIF will increase when the applied electric field shifts from negative to positive, which indicates that fracture may be promoted by a positively applied electric field and inhibited by a negatively applied electric field. This conclusion for the dynamic crack propagation is in agreement with the static experimental observations as well as the prediction by local energy release rate for cracked piezoelectric ceramics (Gao et al., 1997).

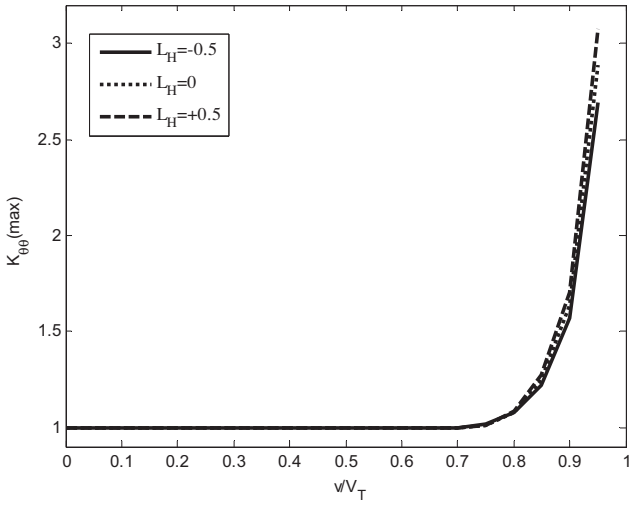

Fig. 9a. The maximum HSIFs versus v/V_T for different magnetic induction loading L_H when $L_E = 0$.

The effect of magnetic loading on the variation of HSIF with angle θ when $L_E = 0$ and $v/V_T = 0.7$ is shown in Fig. 7. It is observed that the maximum value of HSIF at the angles $\theta \neq 0$ will increase as the applied magnetic field shifts from negative to positive, which means that a positive magnetic field loading may promote fracture and a negative magnetic field loading may inhibit fracture. The comparison of Fig. 7 with Fig. 6 shows that the magnetic loading parameter L_H have less influence on the values of HSIFs and kinking angels than the electric loading parameter L_E with the same value. The particular material properties used in the computation determine different response will occur when certain electric or magnetic loading is applied to the cracked body, and the contribution of the electric and magnetic loadings of certain values to the stress field is quite different.

The variation of the normalized maximum HSIFs with crack speed v/v_T for different electric field loading L_E when $L_H = 0$ is shown in Fig. 8a, and the corresponding angles at which the maximum HSIFs appear are shown in Fig. 8b. It can be seen that the magnitude of the maximum HSIFs tends to increase as the crack speed increases when it is larger than a certain value ($v/v_T \approx 0.7$). The crack tends to propagate along the original crack plane when $v/v_T < 0.7$ as the maximum hoop stress intensity factor occurs at the angle $\theta = 0$, which, agrees with the numerical results by Zhu and Yang (1999) for the crack kinking in a piezoelectric solid. Fig. 8b shows that the crack kinking angle increases as the crack speed increases when $v/v_T > 0.7$, and positive electric field loading will lead to larger kinking angle than the negative electric field loading. It should be noted that two symmetric kinking angles exist due to the fact that the stress distribution around the crack tip is symmetric about the crack face, which means that the crack bifurcation phenomena may be observed.

The variation of the normalized maximum HSIFs with crack speed v/v_T for different magnetic field loading L_H is shown in Fig. 9a when $L_E = 0$, and the corresponding angles at which the maximum HSIFs appear are shown in Fig. 9b. It is observed that the magnetic field loading L_H affects the values of the HSIFs and the corresponding kinking angles.

The variation of crack kinking angles versus L_E for different crack speed v/V_T when $L_H = 0$ is displayed in Figs. 10a and 10b shows the crack kinking angles versus the magnetic loading parameter L_H at different crack speed v/V_T when $L_E = 0$. When the crack speed $v/V_T \leqslant 0.6$, the crack will not kink under mechanical and pure electric loadings as the maximum hoop stress occurs at the original crack plane direction. When the crack speed is high

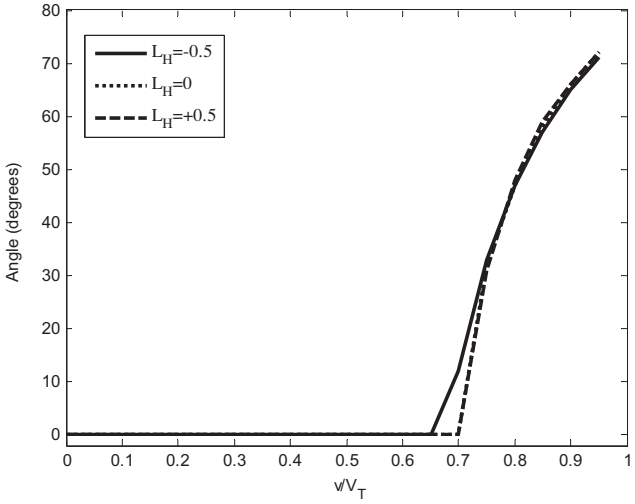

Fig. 9b. The crack kinking angles versus v/V_T for different L_H when $L_E = 0$.

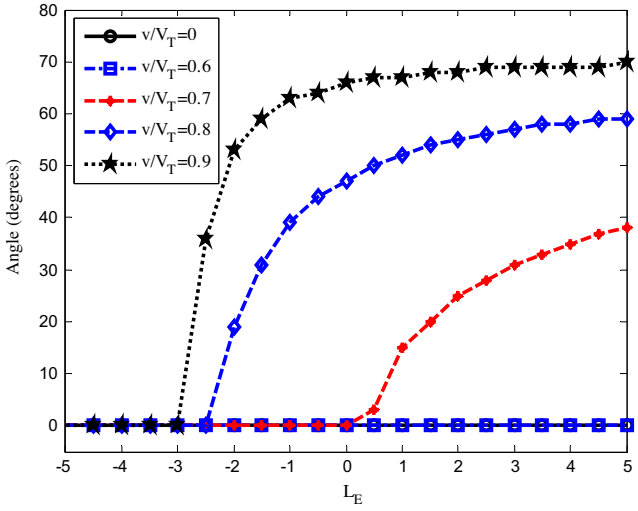

Fig. 10a. The crack kinking angles versus L_E for different v/V_T when $L_H = 0$.

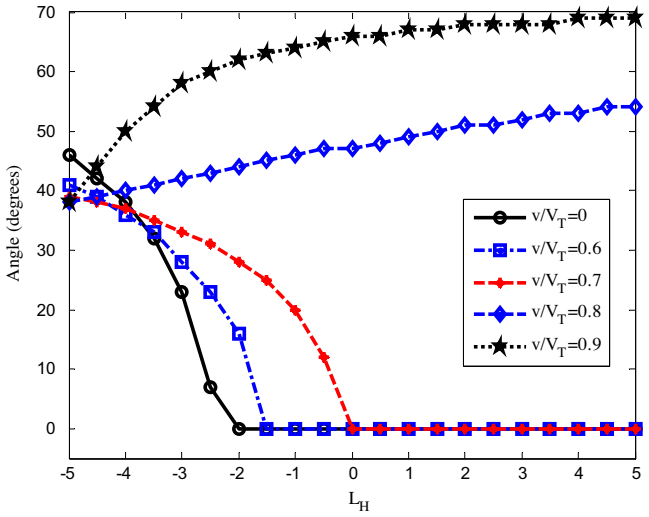

Fig. 10b. The crack kinking angles versus L_H for different v/V_T when $L_E = 0$.

enough, say, $v/V_T \geqslant 0.7$, positive electric loading may lead to more possibility of crack kinking than negative electric loading, and the corresponding kinking angles increase as the crack speed increases. The smallest value of that the propagating crack may kink decreases as the crack speed increases when crack moves fast enough ($v/V_T \geqslant 0.7$). From Fig. 10b we can see that negative values of the magnetic loading may lead to crack kinking when $v/V_T \leqslant 0.7$ and $L_E = 0$, and positive magnetic loading may not cause crack kinking. The smallest value (absolute value) for that may lead to crack kinking decreases as the crack speed increases as $v/V_T \leqslant 0.7$. The crack kinking angles increase as the magnetic loading increases when the crack speed is high enough, as shown in Fig. 10b.

The energy release rate of an impermeable crack in a magento-electroelastic material is negative regardless of positive or negative electric and magnetic loadings in the absence of the mechanical loading (Zhong and Li, 2007), and this conclusion indicates that the prediction of crack kinking phenomenon may be different from that by using the stress intensity factor criterion. It is noted that there are no any experimental observations or results found for dynamic crack propagation in magnetoelectroelastic materials. Experimental work is indeed important to verify the theoretical results, and only experiments may tell which criterion is suitable for prediction of crack kinking (Azhdari and Nemat-Nasser, 1996a).

The authors believe that it is straightforward to extend the method used in this paper to study the dynamic mode II crack problem in magnetoelectroelastic materials, and this will be an interesting topic for future work.

6. Concluding remarks

A constant moving crack in an infinite, magnetoelectroelastic material under in-plane mechanical, electric and magnetic loading is studied for impermeable crack surface boundary conditions. Fourier transforms are applied to reduce the mixed boundary value problem of the crack to dual integral equations, which are solved exactly. Asymptotic fields near the crack tip are obtained in an explicit form and the corresponding field intensity factors are defined. The crack kinking phenomenon is investigated by applying the maximum hoop stress intensity factor criterion. Numerical result indicates that the crack speed and the electric and magnetic loading have influence on the singular field distributions around the crack tip. The magnitude of the maximum HSIF tends to increase as the crack speed increases when it is larger than a certain value. The crack kinking angles for the impermeable crack boundary conditions are numerically determined for the moving crack under electric and magnetic loading.

Appendix A

The constants in Eq. (15) are defined as

$$\begin{aligned}\Pi_1 &= (P_0 + e_{33}E_0 + h_{33}H_0)/C_{33}\\ \Pi_2 &= -E_0\\ \Pi_3 &= -H_0\end{aligned} \tag{A.1}$$

$$\begin{Bmatrix} a_j \\ b_j \\ d_j \end{Bmatrix} = \begin{bmatrix} C_{11v} - C_{44}\gamma_j^2 & e_{31} + e_{15} & h_{31} + h_{15} \\ (C_{13} + C_{44})\gamma_j^2 & e_{33}\gamma_j^2 - e_{15} & h_{33}\gamma_j^2 - h_{15} \\ (e_{31} + e_{15})\gamma_j^2 & \lambda_{11} - \lambda_{33}\gamma_j^2 & d_{11} - d_{33}\gamma_j^2 \end{bmatrix}^{-1} \times \begin{Bmatrix} C_{13} + C_{44} \\ C_{33}\gamma_j^2 - C_{44v} \\ e_{33}\gamma_j^2 - e_{15} \end{Bmatrix}, \quad (j = 1 - 4) \tag{A.2}$$

where

$$C_{11v} = C_{11} - \rho v^2, \quad C_{44v} = C_{44} - \rho v^2 \tag{A.3}$$

The constants σ_0, D_0, B_0 are defined as

$$\begin{Bmatrix} \sigma_0 \\ D_0 \\ B_0 \end{Bmatrix} = \begin{bmatrix} C_{13} & e_{31} & h_{31} \\ e_{33} & -\lambda_{33} & -d_{33} \\ h_{33} & -d_{33} & -\mu_{33} \end{bmatrix} \begin{bmatrix} C_{33} & e_{33} & h_{33} \\ 0 & -1 & 0 \\ 0 & 0 & -1 \end{bmatrix}^{-1} \begin{Bmatrix} P_0 \\ E_0 \\ H_0 \end{Bmatrix} \tag{A.4}$$

References

Azhdari, A., Nemat-Nasser, S., 1996a. Energy-release rate and crack-kinking in anisotropic brittle solids. J. Mech. Phys. Solids 44, 929–951.

Azhdari, A., Nemat-Nasser, S., 1996b. Hoop stress intensity factor and crack-kinking in anisotropic brittle solids. Int. J. Solids Struct. 33, 2023–2037.

Chen, Z.T., Yu, S.W., 1997. Antiplane Yoffe crack problem in piezoelectric materials. Int. J. Fract. 84, L41–L45.

Chen, Z.T., Karihaloo, B.L., Yu, S.W., 1998. A Griffith crack moving along the interface of two dissimilar piezoelectric materials. Int. J. Fract. 91, 197–203.

Copson, E.T., 1961. On certain dual integral equations. Proc. Glasgow Math. Assoc. 5, 19–24.

Craggs, J.W., 1960. On the propagation of a crack in an elastic-brittle material. J. Mech. Phys. Solids 8, 66–75.

Fabrikant, V.I., 2003. Computation of infinite integrals involving three Bessel functions by introduction of new formalism. Z. Angew. Math. Mech. 83, 363–373.

Feng, W.J., Pan, E., Wang, X., 2007. Dynamic fracture analysis of a penny-shaped crack in a magnetoelectroelastic layer. Int. J. Solids Struct. 44, 7955–7974.

Freund, L.B., 1972. Crack propagation in an elastic solid subjected to general loading-I. Constant rate of extension. J. Mech. Phys. Solids 8, 129–140.

Frund, L.B., 1990. Dynamic Fracture Mechanics. Cambridge University Press, New York.

Gao, H., 1993. Surface roughening and branching instabilities in dynamic fracture. J. Mech. Phys. Solids 41, 457–486.

Gao, H., Zhang, T.-Y., Tong, P., 1997. Local and global energy release rates for an electrically yielded crack in a piezoelectric ceramics. J. Mech. Phys. Solids 45, 491–509.

Gao, C.F., Hannes, K., Herbert, B., 2003. Crack problems in magnetoelectroelastic solids. Part I: exact solution of a crack. Int. J. Eng. Sci. 41, 969–981.

Herrmann, K.P., Loboda, V., 2006. Contact zone approach for a moving interface crack in a piezoelectric bimaterial under thermoelectromechanical loading. Arch. Appl. Mech. 75, 665–677.

Hu, K.Q., Li, G.Q., 2005a. Constant moving crack in a magnetoelectroelastic material under anti-plane shear loading. Int. J. Solids Struct. 42, 2823–2835.

Hu, K.Q., Li, G.Q., 2005b. Electro-magneto-elastic analysis of piezoelectromagnetic strip with a finite crack under longitudinal shear. Mech. Mater. 37, 925–934.

Hu, K.Q., Zhong, Z., 2005. A moving mode-III crack in a functionally graded piezoelectric strip. Int. J. Mech. Mater. Des. 2, 61–79.

Hu, K.Q., Kang, Y.L., Li, G.Q., 2006. Moving crack at the interface between two dissimilar magnetoelectroelastic materials. Acta Mech. 182, 1–16.

Huang, J.H., Kuo, W.-S., 1997. The analysis of piezoelectric/piezomagnetic composite materials containing ellipsoidal inclusions. J. Appl. Phys. 81, 1378–1386.

Kwon, S.M., Lee, K.Y., 2001. Constant moving crack in a piezoelectric block: anti-plane problem. Mech. Mater. 33, 649–657.
Lekhnitskii, S.G., 1963. Theory of Elasticity of an Anisotropic Elastic Body. Holden-Day Inc., San Francisco.
Li, X.F., 2005. Dynamic analysis of a cracked magnetoelectroelastic medium under antiplane mechanical and inplane electric and magnetic impacts. Int. J. Solids Struct. 42, 3185–3205.
Li, X.F., Lee, K.Y., 2004. Three-dimensional electroelastic analysis of a piezoelectric material with a penny-shaped dielectric crack. J. Appl. Mech. 71, 866–878.
Li, Y.D., Lee, K.Y., 2010. Collinear unequal crack series in magnetoelectroelastic materials: mode I case solved via new real fundamental solutions. Eng. Fract. Mech. 77, 2772–2790.
Li, S.F., Mataga, P.A., 1996a. Dynamic crack propagation in piezoelectric materials-part I. Electrode solution. J. Mech. Phys. Solids 44, 1799–1830.
Li, S.F., Mataga, P.A., 1996b. Dynamic crack propagation in piezoelectric materials-part II. Vacuum solution. J. Mech. Phys. Solids 44, 1731–1866.
Li, X.F., Fan, T.Y., Wu, X.F., 2000. A moving Mode-III crack at the interface between two dissimilar piezoelectric materials. Int. J. Eng. Sci. 38, 1219–1234.
Lin, S., Narita, F., Shindo, Y., 2003. Electroelastic analysis of a penny-shaped crack in a piezoelectric ceramic under mode I loading. Mech. Res. Commun. 30, 371–386.
Ma, C.-C., Lee, J.-M., 2009. Theoretical analysis of generalized loadings and image forces in a planar magnetoelectroelastic layered half-plane. J. Mech. Phys. Solids 57, 598–620.
Piva, A., Tornabene, F., Viola, E., 2007. Subsonic Griffith crack propagation in piezoelectric media. Eur. J. Mech. A/Solids 26, 442–459.
Qin, Q.H., 2005. 2D Green's functions of defective magnetoelectroelastic solids under thermal loading. Eng. Anal. Boundary Elem. 29, 577–585.
Rekik, M., El-Borgi, S., Ounaies, Z., 2012. Anembedded mixed-mode crack in a functionally graded magnetoelectroelastic infinite medium. Int. J. Solids Struct. 49, 835–845.
Rojas-Diaz, R., Garcia-Sanchez, F., Saez, A., Zhang, C., 2007. Fracture analysis of magnetoelectroelastic composite materials. Key Eng. Mater. Adv. Fract. Damage Mech. VI 348–349, 69–72.
Soh, A.K., Liu, J.-X., Lee, K.L., Fang, D.-N., 2002. On a moving Griffith crack in anisotropic piezoelectric solids. Arch. Appl. Mech. 72, 458–469.
Song, Z.F., Sih, G.C., 2003. Crack initiation behavior in a magnetoelectroelastic composite under in-plane deformation. Theor. Appl. Fract. Mech. 39, 189–207.
Stroh, A.N., 1962. Steady state problems in anisotropic elasticity. J. Math. Phys. 41, 77–103.
Suo, Z., Kuo, C.-M., Barnett, D.M., Willis, J.R., 1992. Fracture mechanics for piezoelectric ceramics. J. Mech. Phys. Solids 40, 739–765.
Tian, W.Y., Rajapakse, R.K.N.D., 2005. Fracture analysis of magnetoelectroelastic solids using path independent integrals. Int. J. Fract. 131, 311–335.
Tian, W.Y., Rajapakse, R.K.N.D., 2008. Theoretical model for crack branching in magnetoelectroelastic solids. Int. J. Appl. Electromagnet. Mech. 27, 53–74.
Tupholme, G.E., 2009. Moving antiplane shear crack in transversely isotropic magnetoelectroelastic media. Acta Mech. 202, 153–162.
Wan, Y.P., Yue, Y.P., Zhong, Z., 2012. A mode III crack crossing the magnetoelectroelastic biomaterial interface under concentrated magnetoelectromechanical loads. Int. J. Solids Struct. 49, 3008–3021.
Wang, B.-L., Mai, Y.-W., 2007. Applicability of crack-face electromagnetic boundary conditions for fracture of magnetoelectroelastic materials. Int. J. Solids Struct. 44, 387–398.
Willis, J.R., 1967. Crack propagation in viscoelastic media. J. Mech. Phys. Solids 8, 229–240.
Yang, W., 2002. Mechatronic Reliability: Electric Failures, Mechanical-Electrical Coupling, Domain Switching, Mass-Flow Instabilities. Springer Verlag, New York.
Yang, W., Suo, Z., Shin, C.F., 1991. Mechanics of dynamic debonding. Philos. Trans. R. Soc. London A 433, 679–697.
Yoffe, E.H., 1951. The moving Griffith crack. Philos. Mag. 42, 739–750.
Zhao, M.-H., Fan, C.-Y., 2008. Strip electric-magnetic breakdown model in magnetoelectroelastic medium. J. Mech. Phys. Solids 56, 3441–3458.
Zhao, M.-H., Wang, H., Yang, F., Liu, T., 2006a. A magnetoelectroelastic medium with an elliptical cavity under combined mechanical-electric-magnetic loading. Theor. Appl. Fract. Mech. 45, 227–237.
Zhao, M.-H., Yang, F., Liu, T., 2006b. Analysis of a penny-shaped crack in a magnetoelectroelastic medium. Philos. Mag. 86, 4397–4416.
Zhong, X.C., Li, X.F., 2007. Magnetoelectroelastic analysis for an opening crack in a piezoelectromagnetic solid. Eur. J. Mech. A/Solids 26, 405–417.
Zhong, X.C., Li, X.F., 2008. Fracture analysis of a magnetoelectroelastic solid with a penny-shaped crack by considering the effects of the opening crack interior. Int. J. Eng. Sci. 46, 374–390.
Zhou, Z.G., Chen, Z.T., 2008. Fracture mechanics analysis of a partially conducting mode I crack in piezoelectromagnetic materials. Eur. J. Mech. A/Solids 27, 824–846.
Zhu, T., Yang, W., 1999. Crack kinking in a piezoelectric solid. Int. J. Solids Struct. 36, 5013–5027.